An Acad Bras Cienc (2024) 96(1): e20230005 DOI 10.1590/0001-3765202420230005
Anais da Academia Brasileira de Ciências | *Annals of the Brazilian Academy of Sciences*
Printed ISSN 0001-3765 I Online ISSN 1678-2690
www.scielo.br/aabc | www.fb.com/aabcjournal

GEOSCIENCES

Distribution of gamma-ray elements in Cerro do Jarau impact structure and a proposal of geothermal modeling

DIEGO D. GARCIA, EMILSON P. LEITE, MARCOS ALBERTO R. VASCONCELOS, EVANGELOS CHRISTOU & ALVARO P. CRÓSTA.

Abstract: Large meteorite impacts release kinetic energy that induces rock deformation, high temperatures and fluid circulation during the cratering process. To understand the correlation between rock deformation and fluid circulation, it is relevant to investigate post-impact hydrothermal flux and its relation to the local geology. The Cerro do Jarau impact structure is a ~13.5 km diameter impact structure located in southern Brazil and formed on Cretaceous continental flood basalts of the Serra Geral Formation and underlying sedimentary strata. This study collected ground gamma-ray data over the structure and produced K, eTh and eU concentrations, eTh/K ratio and F-factor maps to characterize it in terms of its radiometric signatures and their respective spatial distribution. A general decrease in the concentration of the three elements was observed from the outer-rim towards the center of the crater. The central area is defined by very low radiometric values, with relatively high K values, thus indicating the occurrence of K-bearing rocks. Numerical simulations using the HYDROTHERM 3 code showed the fluid circulation pattern over the impact structure. Data interpretation resulted in a scenery consistent with potential fluid remobilization within the impact structure related to hydrothermal processes in the late stages of the crater formation process.

Key words: gamma ray spectrometry, hydrothermal alteration, impact crater, numerical modeling.

INTRODUCTION

Terrestrial impact structures formed in volcanic rocks of basaltic composition can provide important constraints to understand the effects of meteorite impacts on the surfaces of other planetary bodies (French 1998, Crósta 2008). The Cerro do Jarau structure (CJ) was formed in a Paleozoic predominantly volcanic sequence of the Paraná Basin, the Serra Geral Formation (Figure 1). CJ has a nearly circular shape with a diameter of ~13.5 km, and exhibits morphologic concentric rings characterized by topographic depressions in its outer and centermost portions (Crósta et al. 2010). Cerro do Jarau structure can be classified as a complex type crater, due to its circular feature and also due to the morphological set of concentric rings around a central uplifted core.

Crósta et al. (2010) identified the occurrence of parautochthonous monomict lithic impact breccia and polymict impact breccias, as well as striated joint surfaces resembling crude shatter cones in sandstones and basalts. They also reported the presence of rare planar fractures (PF) in quartz clasts in the polymict breccias. No occurrence of shatter cones has been reported yet on the CJ. Sanchez et al. (2014) related the occurrence of sandstones at the center of CJ to a possible local sedimentary basin model based

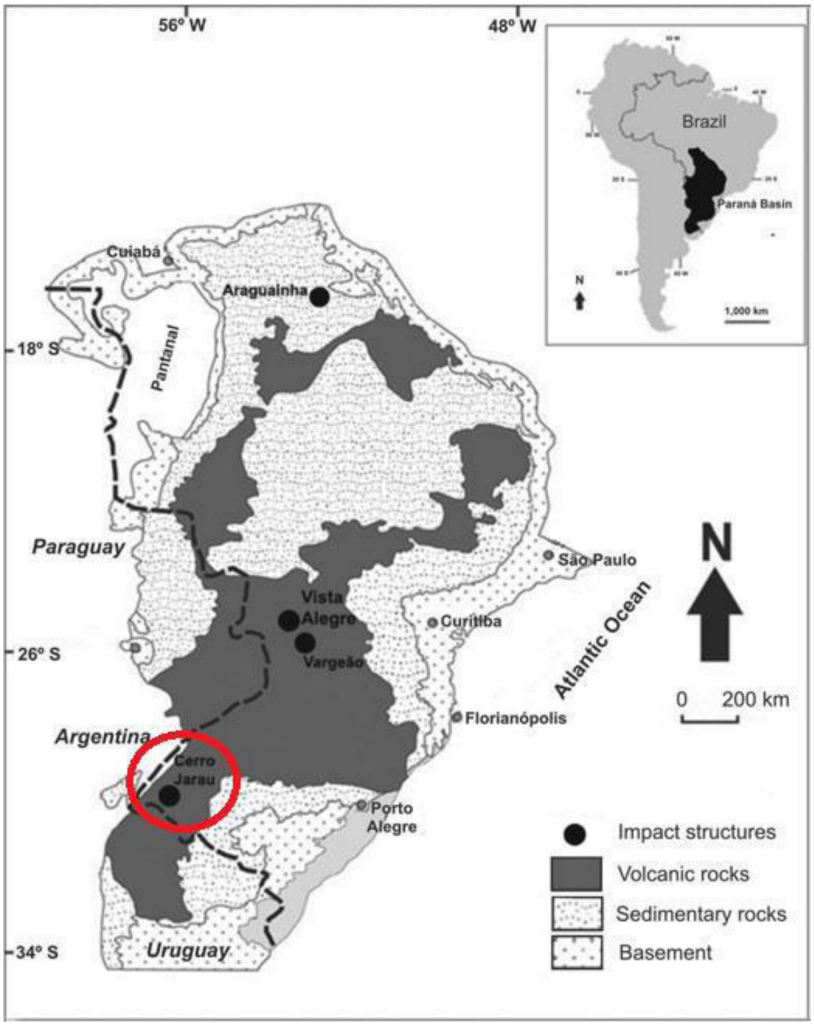

Figure 1. Impact structures in the PB (extracted from Crósta et al. 2010). Red circle indicates the location of the CJS.

on the geometry of the observed geological structures, a structural model that is not compatible with an impact structure of such dimension as proposed by Crósta et al. (2010).

Bona-fide evidence for the impact origin of CJ was presented by Reimold et al. (2019), by means of sets of PF, PDF and FF (feather features) in quartz grains from the deformed sandstone from the center of the structure. The presence of these micro-deformation features is used as a robust demonstration of the impact origin of a potential crater and it is, therefore, conclusive (French 1998, French & Koeberl 2010, Poelchau & Kenkmann 2011).

As no underground data are available for CJ (i.e., no drill cores), an effort to conduct a comprehensive geophysical characterization of CJ was started a few years ago. The first approach was carried out through a gravity survey that investigated the structural uplift based on the Bouguer anomaly (Giacomini et al. 2017). Their results overruled the bowl-shaped basin model proposed by Sanchez et al. (2014).

In geophysics, the analysis of the spatial distribution of gamma-ray elements is employed to support geological mapping, and also to identify potential areas of hydrothermal activity. Galbraith & Saunders (1983) showed that gamma-ray measurements are capable

of distinguishing different lithologies and the degree of regional U enrichment, or depletion. Pires (1995) used airbone gamma-ray data, especially the K channel, to identify areas that underwent hydrothermal alteration. Shives et al. (2000) used gamma-ray spectrometry to measure and map K enrichment related to hydrothermal alteration in volcanic-hosted massive sulfide, polymetallic and porphyry mineralization.

An impact event can induce optimal conditions for the circulation of hydrothermal fluids. After an impact, part of the energy released is transformed into mechanical deformation and damage. The remaining energy heats the rocks producing melt, especially in the central uplift region where previously deeper located rocks are brought closer to the surface (Melosh & Ivanov 1999). Such thermal effects result in hydrothermal fluid flows that form new mineral assemblages, resulting in hydrothermal alteration (Reimold et al. 2005, Pirajno 2005, 2009). Examples of hydrothermal alteration associated with impact events can be found in Allen et al. (1982), Newsom et al. (1986), Ames et al. (1998), Osinski & Spray (2001), Naumov (2002), Hagerty & Newsom (2003), Osinski (2005), Schmieder & Kring (2020) and Kring et al. (2021). Thus, the interior of an impact structure, particularly its central area, usually exhibit more or less extensive changes that cause minerals and metals to dissolve and precipitate, depending on the local thermal gradients (Puura & Plado 2004).

Vasconcelos et al. (2012) presented the gamma-ray signatures of the Serra da Cangalha impact structure, showing that K anomalies are likely related to hydrothermal alteration, and provide information that allow to distinguish zones within the structure and to understand the hydrothermal enrichment processes produced by the impact event. Recently, Lamali et al. (2020) applied gamma-ray spectrometry to map lithological units at the Maâdna potential impact structure in Algeria. Niang et al. (2021) employed gamma-spectrometry in Bosuntwi impact structure to state that the circular feature, forming a double ring with high K concentrations, coinciding with the crater rim and a distal ejecta ridge, is not related to hydrothermalism, but it is a function of bedrock lithology.

We present the results of a gamma-ray spectrometric investigation of CJ and its correlation with the local geology. We associated the spatial distribution of K, eU and eTh, as well as the ratio eTh/K, with the local lithological units, and compared the anomalies of these elements with the mineralogy of bedrock lithotypes. Additionally, we developed numerical models to simulate the post-impact conditions within the crater from postulated initial thermodynamic conditions, such as temperature, pressure, and enthalpy distributions. The results of the simulation were post-processed, interpreted, and correlated with the gamma-ray results and with ancillary geological data available for CJ. These results were then employed to evaluate and determine reliable post-impact scenarios, and to establish the duration of hydrothermal circulation associated with the impact event. We produced several models, varying only the permeability of the target rocks. From these outcomes, we obtained the information to analyze whether the distribution of the gamma-ray elements within CJ is lithologically-controled, or driven by the hydrothermal circulation.

GEOLOGICAL SETTING

Crósta et al. (2010) described the CJ as a near-circular feature with a diameter of ~13.5 km, with subdued rim and an inner silicified collar of sandstone, forming annular ridges raising ca. 200 m above the outer plains (known as "pampa" landscape). The structure was formed

on two rock types (basalt and sandstone), both exhibiting some degree of deformation within CJ, in contrast with undeformed basalt flows occurring outside of the outer rim of the structure.

The first evidence to support the impact origin of CJ is the report of brecciation of sandstones and basalt, as well as deformation features in these two rock types (Crósta et al. 2010). The general deformation of local lithologies, combined with striated features resembling shatter cones, planar fractures in quartz grains and occurrence of non-volcanic clastic breccias, led the authors to propose that the CJ was formed by a meteorite impact in the Mesozoic, after the Cretaceous volcanic Serra Geral event (dated at ca. 134.6 ± 0.6 Ma, Thiele & Vasconcelos 2010). Within CJ, Crósta et al. (2010) identified six different lithotypes. Three of them are associated with stratigraphic units of the Paraná Basin: fluvial sandstones of the Guará Formation; aeolian sandstones of the Botucatu Formation; and basalts of the Serra Geral Formation. According to Scherer & Lavina (2005, 2006), both, Guará Formation and sandstones of the Botucatu Formation, were formed from Late Jurassic to Early Cretaceous. The other three lithotypes are: monomict breccias in sandstones; monomict breccias in basalts; and polymict breccias with fragments of both lithologies.

The Serra Geral Formation is mainly composed of horizontal layered basalt flows related to the Paraná-Etendeka Large Igneous Province (LIP) (Peate 1997). Within CJ, they exhibit textural variations that mark contacts among different basaltic lava flows. The contacts commonly exhibit non-horizontal altitudes due to deformation. They have an aphanitic to phaneritic matrix with phenocrystals of plagioclase and augite and rare crystals of magnetite and rutile (Sanchez et al. 2014).

Igneous breccias of varied textures, with clasts that can reach up to 30 cm in diameter, surround the center of CJ. Based on the lack of cataclastic features and on the geometry concordant with the basalts, Sánchez et al. (2014) interpreted them as the product of volcanic processes. On the other hand, due to its unusual angular pattern and its clastic matrix, Crósta et al. (2010) interpreted some of these breccias as possible impact breccias.

Sandstones of the Botucatu Formation (Crósta et al. 2010, Phillip et al. 2010) form the central uplift area of the impact structure, represented by annular ridges. In general, they are intensely silicified, forming the highest local elevations. Layers of plane-parallel stratification, ranging from decimeter to meter, and cross laminating layers of medium to large size, are found (Crósta et al. 2010, Sanchez et al. 2014). Laminated deformed sandstones occur in the innermost area of the structure and they are characterized by laminations of 0.5 to 2.0 cm marked by bands with predominance of quartz alternated by quartz and clay bands and clay bands. These alternating bands indicate oscillation in the sedimentation process deposition (Sanchez et al. 2014). According to Crósta et al. (2010), plane-parallel lamination is typical of fluvial environment and characteristic of the Guará Formation.

Shock microdeformation, including planar fractures (PF), feather features and, in four cases, planar deformation features (PDF), were found in about a dozen of sandstone samples from this part of the structure (Reimold et al. 2019). According to these authors, PF occur in three sets of different orientations in selected quartz grains, FF occur in three orientations per host grain, and PDF were noted in two grains in two orientations each, whereas a dozen other grains showed only single sets of PDF.

According to the stratigraphy proposed by Crósta et al. (2010), the exposure of the sedimentary strata related to the Guará and Botucatu formations, surrounded by the younger basalt of the Serra Geral Formation, indicates local occurrence of a structural uplift at the center of the CJ, differently from the basin model proposed by Sanchez et al. (2014).

DATA PROCESSING AND METHODOLOGY

Gamma-ray

Among the radioactive elements that are natural source of gamma-rays, there are: (i) potassium (K), which is monitored by gamma rays emitted by the isotope K^{40} with an energy peak at 1.46 MeV; (ii) uranium (U), whose isotopes U^{238} and U^{235} do not emit gamma-rays, but the Bi^{214} isotope that is part of their radioactive decay series emits gamma-rays with an energy peak at 1.76 MeV; (iii) thorium (Th), which occurs naturally in the form of the Th^{232} isotope, wherein the Tl^{208} isotope that is part of its decay series emits gamma-ray with an energy peak at 2.62 MeV. Through the detection of gamma-rays emitted by the material after radioactive decay, gamma-ray spectrometry provides estimates of the concentration of the elements K, eU and eTh. eU and eTh. Concentrations are estimated indirectly by counting gamma-rays emitted from isotopes of Bi and Tl, respectively (e.g. Telford et al. 1990).

The field data included gamma-ray spectrometric measurements at 438 locations within the inferred boundaries of the CJ (Garcia D.D., unpublished data, Garcia & Leite 2023). Measurements were made on outcrops along existing roads using a RS-230 portable gamma-ray spectrometer. The data acquistion and the equipment calibration followed the procedure described in Leite et al. (2022).The interpretation of gamma-ray data was carried out using false-color maps of K (Figure 4a), eTh (Figure 4b), eU (Figure 4c), ratio eTh to K (Figure 4d), and ternary map, with K, eTh and eU represented in red, green and blue, respectively. (Figure 6).

Numerical modeling

The code HYDROTHERM (HYDROTHERM Interactive – Version 3.2.0 (HTI); Hayba & Ingebritsen 1994), developed by the United States Geological Survey (USGS), was used to model the impact-induced hydrothermal activity in CJ structure. HYDROTHERM is a suitable code for modeling convective and conductive water and heat transport in terrestrial and Martian impact craters (e.g. Rathbun & Squyres 2002, Abramov & Kring 2004, 2005, 2007, Sanford 2005). It was employed to explore the hydrothermal fluid circulation in the CJ geological setting following the crater formation.

The governing equations used in the current version of the HTI code are expressions of mass and energy conservation that are posed in terms of pressure and enthalpy (Ingebritsen & Hayba 1994, Hayba & Ingebritsen 1994). The code incorporates data from various sources to develop consistent equations of state (EoS) for conditions ranging from 0°C to 1200°C and from 0.5 to 10 kbar (50 KPa to 1 GPa). The EoS are formulated in HTI using a standard finite-difference approach. The equations, however, are strongly coupled and highly nonlinear, because variables such as relative permeability, density, and viscosity vary widely with pressure and enthalpy (Hayba & Ingebritsen 1994). A three-dimensional iterative technique based on the general conjugate residuals (GMRES) method is a new functional characteristic of the HTI version 3 code, and this new solution is over 10 times faster for solving this problem than the original HT code. Further details on the EoS are provided in the HT v.3 user's manual (USGS). The Fortran source code of HYDROTHERM

(HT) version 3 and its accompanying documents and files are publicly available and can be downloaded from https://volcanoes.usgs.gov/software/hydrotherm/.

Our computational scenarios were based on prior work by Abramov & Kring (2004, 2005, 2007), Sanford (2005), Borović et al. (2019). They have previously constrained the hydrous circulation in a variety of Martian and terrestrial impact-induced, volcanic and geothermal aquifers, therein deriving the lifetime of the fluid flows. The simulations focused primarily on determining the temperature distributions, water-, steam- and supercritical fluid- mass flux, heat flux, pressure and enthalpy in CJ. Fluid flows of T > 500 °C are characterized as super-critical mass fluxes and 2-phase (water-steam) mass fluxes, and these flows commonly produce specific mineral assemblages. Such assemblages comprise pyrite, anhydrite, prehnite, pyrrhotite and zeolites that are often present in rocks retrieved from impact craters. Shocked quartz grains are also observed in some of the investigated samples (Reimold et al. 2019). Finally, the abundance of mineral assemblages and isotopic compositions observed in impact-related rocks can approve or reject the computed distributions of temperature, pressure and fluid flows that the HTI code produces.

Therefore, in this study, numerical modelling results were compared and coupled with previous stratigraphic, 3D gravitational models (Giacomini et al. 2017), and the gamma-ray spectrometric data here presented, to evaluate the robustness of the numerical simulations and to establish a holistic and vigorous model for the potential initiation and evolution of the hydrothermal circulation in CJ following the impact event.

To compare and examine the hydrothermal response in CJ using a variety of thermodynamic scenarios, eight simulations were conducted using different petrophysical parameters for the local lithologies. Starting from the boundary conditions of the simulations (Figure 3), the input parameters were defined by the HTI interactive programming environment. A geological setting of a 13.8 km horizontal distance and a maximum depth of 3.5 km from the surface were designed in 2D using the HTI interface on a grid of 150 × 40 cells. This parameterization was applied according to the geological map suggested by Crósta et al. 2010 (Figures 2 of this work). The 3.5 km depth of the grid in our numerical models was based on iSALE simulations performed for small impact-cratering systems, as described in Jõeleht et al. (2005), and references therein. The grid resolution was determined by trial-and-error, in order to reach the maximum possible resolution for this simulation environment, and was achieved after several computational experiments with different resolutions.

The chosen resolution of the grid (6000 cells) in the numerical models of this work is the maximum resolution that could have been achieved according to the processing capacity of the computational facilities at the University of Glasgow, and represents very high detail of geophysical modelling. For comparison, Abramov & Kring (2007) used a very high resolution of 9900 cells in HT simulations for the Chicxulub crater, which is a 160 km in diameter crater (2D grid: 160 km horizontal distance, and 7 km vertical distance; in Abramov & Kring (2007)). In this work, we introduced the maximum achievable resolution of 6000 cells for CJ which is an impact structure of just 13.8 km (2D grid: 13.8 km distance and 3.5 km depth). Conclusively, by ''trial and error', we mean that simulation experiments were performed by testing lower resolutions initially, and by then gradually increasing the resolution of the grid to achieve the highest possible resolution, accuracy and detail for our hydrothermal models. Hence, the threshold of

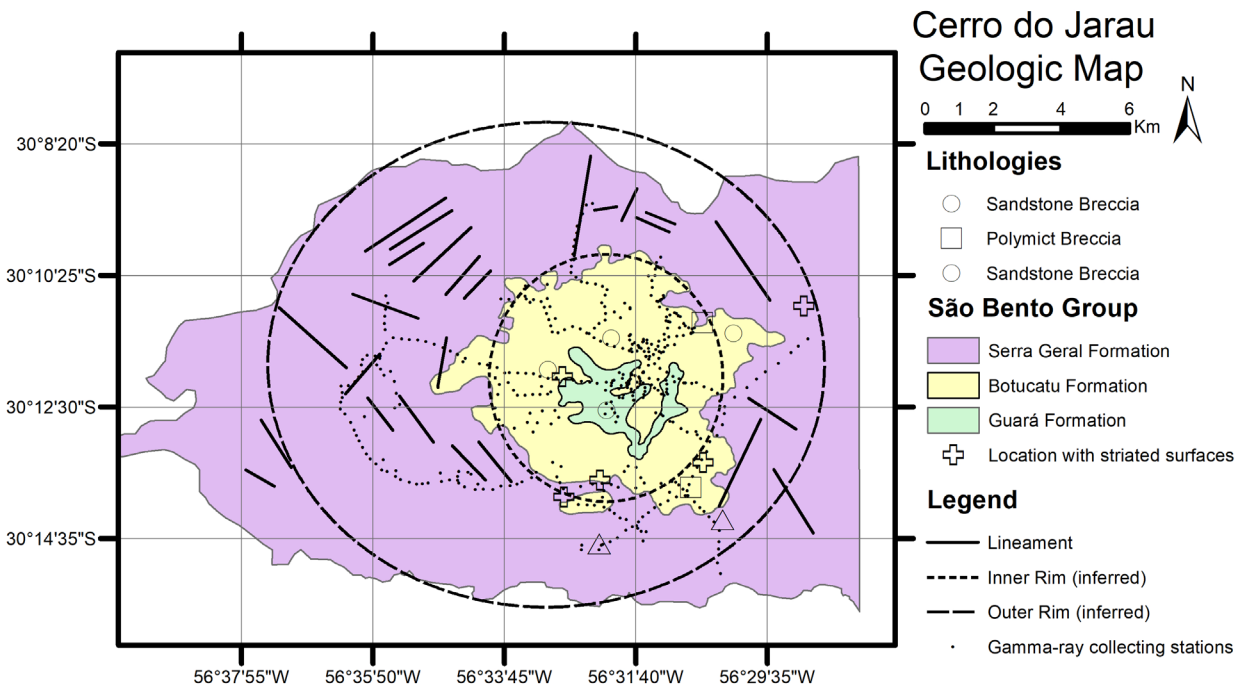

Figure 2. Geological map of the CJS showing the distribution of the gamma-ray data points acquired in this study. (Modified from Crósta et al. 2010).

6000 blocks is the maximum possible resolution that could have been used for the HT simulation grid of CJ.

Two different lithostratigraphic settings were used for the boundary conditions (Supplementary Materials – Fig. S1 and S10) to account for the observed differences in rock distributions between the N-S and W-E geological sections suggested by Giacomini et al. (2017) (see figures S2, S3 and S4 therein indicating the asymmetry of CJ). All the modeled physical properties of the lithological units that comprise CJ are shown in Table I. The initial thermodynamic conditions (temperature, pressure, and enthalpy distributions) after the bolide's impact were programmed in the grid according to experiments and previously published work on the shock physics of small impact-craters (Jõeleht et al. 2005, Timms et al. 2017, and references therein). The temperature contours were designed by the HTI pre-processor, and the input of their spatial distributions and values was established after experimental trials through the HTI post-processor (Fig. S1 - S10).

We primarily examined two different hypotheses for the permeability of the rocks. Since permeability dictates the hydrothermal flow in a geological setting, we first run our simulations considering high-permeability versus low-permeability rock units. Furthermore, as the available geological and geophysical data (Giacomini et al. 2017, and references therein) indicate two different lithostratigraphic distributions and thus, an asymmetry between the N-S and W-E orientation of the brecciated basaltic units in their reconstructed geological cross-sections, two additional hypotheses for the dissimilar lithological distributions were examined in our computations (Fig. S1 and S10).

Finally, due to the fluvial sedimentary lithology present in CJ, we investigated the induced hydrothermal system in the presence and absence of stream flows at the surface of the crater floor, as well as in the outer-rim

Table I. Gama-ray results for each lithology with average, minimun, maximun and standard deviation.

Gamma-ray Elements	Lithology	Average	Minimum	Maximum	Standard Deviation
K (%)	Guará Formation	0.7	0	1.9	0.55
	Botucatu Formation	0.1	0	2.6	0.50
	Serra Geral Formation	0.7	0	2.2	0.56
Th (ppm)	Guará Formation	2.6	0.6	5.1	0.96
	Botucatu Formation	2.1	0.2	10.9	1.52
	Serra Geral Formation	4.7	1.2	10.7	1.82
U (ppm)	Guará Formation	0.8	0	2.2	0.57
	Botucatu Formation	1.1	0	3.3	0.65
	Serra Geral Formation	1.6	0.4	3.7	0.56
Th/K	Guará Formation	3.7	NA	NA	1.76
	Botucatu Formation	21.0	NA	NA	3.04
	Serra Geral Formation	6.7	NA	NA	3.24

and inner-rim fluvial and aeolian sediments. Conclusively, the permeability of the rocks, lithostratigraphic distributions and the presence or absence of stream flows at the surface boundary of the simulation grid resulted in the definition of eight sets of computational scenarios. Of these, all the potential combinations of initial conditions have been tested (see Supplementary Materials, scenarios 1 to 4).

In all simulations, we adjusted a basal heat flux to a value of 60 mW/m² to the bottom boundary of our grid. The top boundary represents aeolian and fluvial sedimentary layers on the surface of which a pressure of 1.01 bar and a temperature of 30°C have been assigned as constant values for initial conditions (Figures S1 and S10). Half the scenarios (4 and 7; in Supplementary Materials) consider a stream influx at the top of the simulation grid and inside the sedimentary layers of the aeolian and fluvial deposits. In those scenarios, the stream flows have been given a temperature of 4°C, and a flow rate of 9.5E+7 kg/yr close to the surface and beyond the structure's rim (outer-rim region). Additionally, an inflow rate of 9.5E+5 kg/yr was used to account for stream flows in the fluvial and aeolian sediments within the inner-rim region of the crater and closer to the inner-slopes of the peak ring (Figures S1 and S10). The chosen values for the hypothetic flow rates in the fluvial and aeolian sediments of CJ derive from average estimates for low hypothetic stream flux (Boano et al. 2014, Gomez-Velez et al. 2015, Galloway et al. 2019) in characterized small river networks (Thoms et al. 2018). However, further environmental research should be conducted to conclude whether a fluvial network could have interacted with the CJ hydrothermal setting after the crater's formation. In our modelling, we have merely experimented with the suggested low hyporheic stream flux to observe its effects on the mechanics of the simulated hydrothermal system.

RESULTS

Distribution of gamma-ray elements

Table II shows the statistics of K, eTh and eU concentrations for each lithological unit. In

Table II. Physical parameters of the geological setting used in the simulations; caption 1a reports on the use of lower permeability rock units in our computational scenarios, while caption 1b considers higher permeability (by one order of magnitude) rock units. The upper table refers to the lower Permeability Computational Scenarios, whereas the lower table refers to the higher Permeability Computational Scenarios.

1a)

Petrophysical Properties	Brecciated Basalt	Brecciated Sandstone	Breccia with Sandstone Clasts	Fluvial & Aeolian Sediments
Permeability (k) {m²}	k_z=f(d,T), k_x=f(d,T)	kz=f(d,T), $k_{x=}$=f(d,T)	k_z=f(d,T), k_x=f(d,T)	k_z=f(d,T), k_x=f(d,T)
Porosity (ϕ) {%}	ϕ=f(d,T)	ϕ=f(d,T)	ϕ=f(d,T)	ϕ=f(d,T)
Thermal Conductivity {W/m*K}	2.7	2.5	2	2
Specific Heat Capacity {J/kg*K}	1000	800	750	700
Density {kg/m³}	2700	2300	2000	1700
Surface Permeability {m²}	9.00E-18	9.00E-17	9.00E-16	9.00E-14
Surface Porosity($\phi_{surface}$)	5.00%	20.00%	25.00%	35.00%

1b)

Petrophysical Properties	Brecciated Basalt	Brecciated Sandstone	Breccia with Sandstone Clasts	Fluvial & Aeolian Sediments
Permeability (k) {m²}	k_z=f(d,T), k_x=f(d,T)	kz=f(d,T), $k_{x=}$=f(d,T)	k_z=f(d,T), k_x=f(d,T)	k_z=f(d,T), k_x=f(d,T)
Porosity (ϕ) {%}	ϕ=f(d,T)	ϕ=f(d,T)	ϕ=f(d,T)	ϕ=f(d,T)
Thermal Conductivity {W/m*K}	2.7	2.5	2	2
Specific Heat Capacity {J/kg*K}	1000	800	750	700
Density {kg/m³}	2700	2300	2000	1700
Surface Permeability {m²}	9.00E-17	9.00E-16	9.00E-15	9.00E-13
Surface Porosity($\phi_{surface}$)	5.00%	20.00%	25.00%	35.00%

general, most K values are between 0.5% – 0.9%, reflecting the three-main outcropping lithological units in the area: Serra Geral Formation, Botucatu Formation and Guará Formation (Figure 4a). Low K values (0% to 0.5%) are found mainly over the Botucatu sandstones that form a central collar surrounding the Guará sandstones, with an average of 0.1%. Such signatures can be explained by the occurrence of aeolian sandstone composed of quartz (90%), feldspar (5%) and secondary minerals (5%) (Crósta et al. 2010, Sanchez 2014).

K values between 0.9% and 2.1% are observed over the sandstones of the Guará Formation, which corresponds to the innermost area of the central uplifted. They present average of 0.7%, and its signature may be associated with the intercalated clays and sands, considering soils over shales usually contains concentration of 1.5% K, and sandstones 1.3% (Dickson & Scott

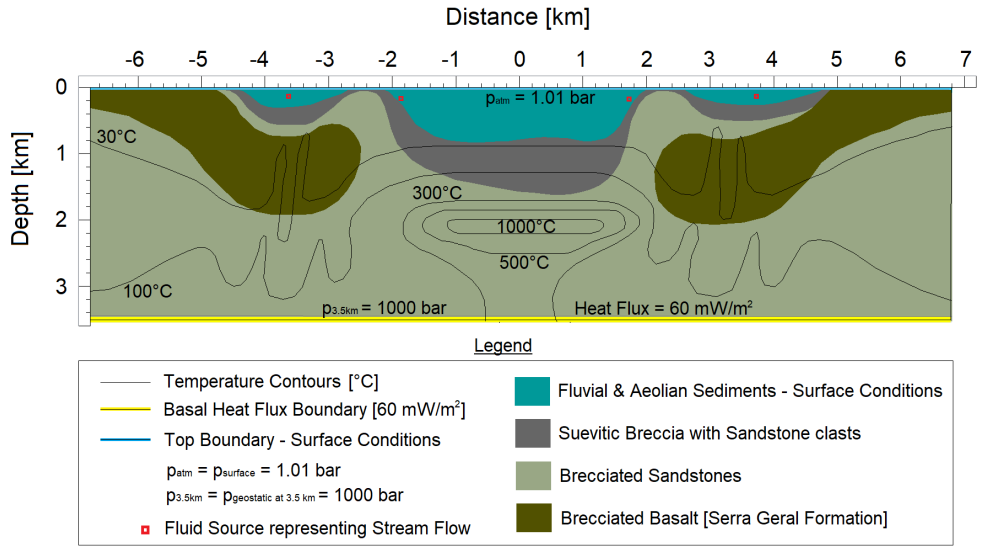

Figure 3. Boundary conditions for the simulation sets 1 to 4 via the HTI code.

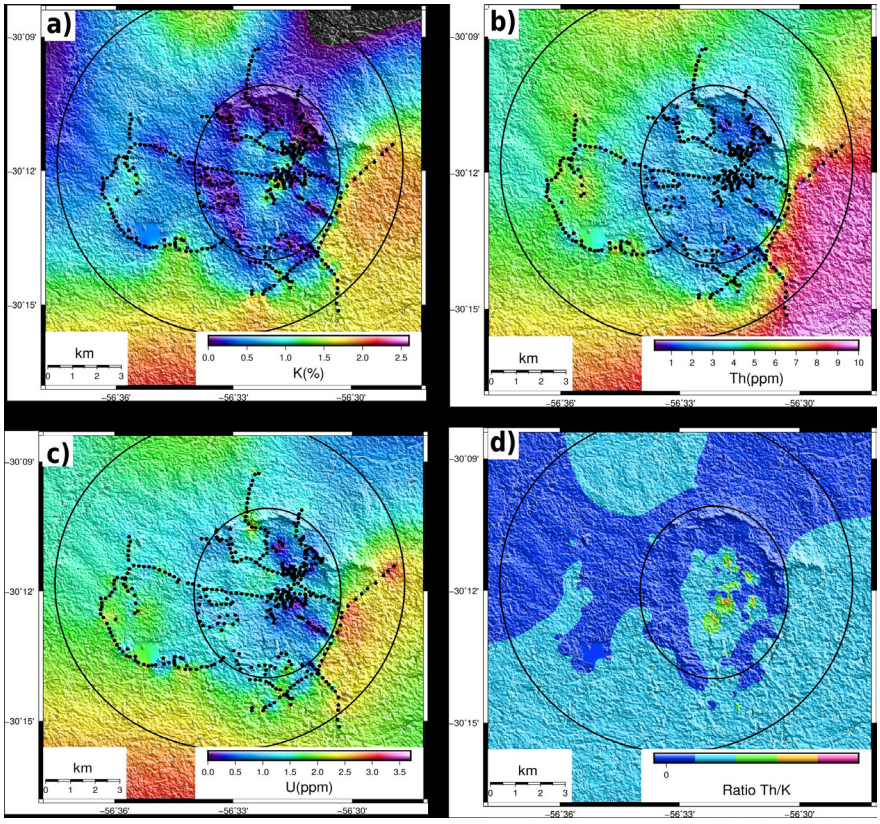

Figure 4. Gamma-ray channels showing distribution of the collecting stations (Garcia D.D., unpublished data) in the Cerro do Jarau impact structure. In (a) K channel; (b) eTh channel; (c) eU channel; (d) eTh/K ratio.

1997). High K values are also observed in the southeastern-side of the structure, over the rocks of the Botucatu Formation (Figure 4a). However, this is not the typical signature of similar sandstones elsewhere within the remaining structure. The entire central uplift area is dominated by those rocks and exhibit predominantly low K (%) values in comparison with the other lithologies.

In the areas where the Serra Geral Formation outcrops the K signature is characterized by low values in comparison with other lithologies.

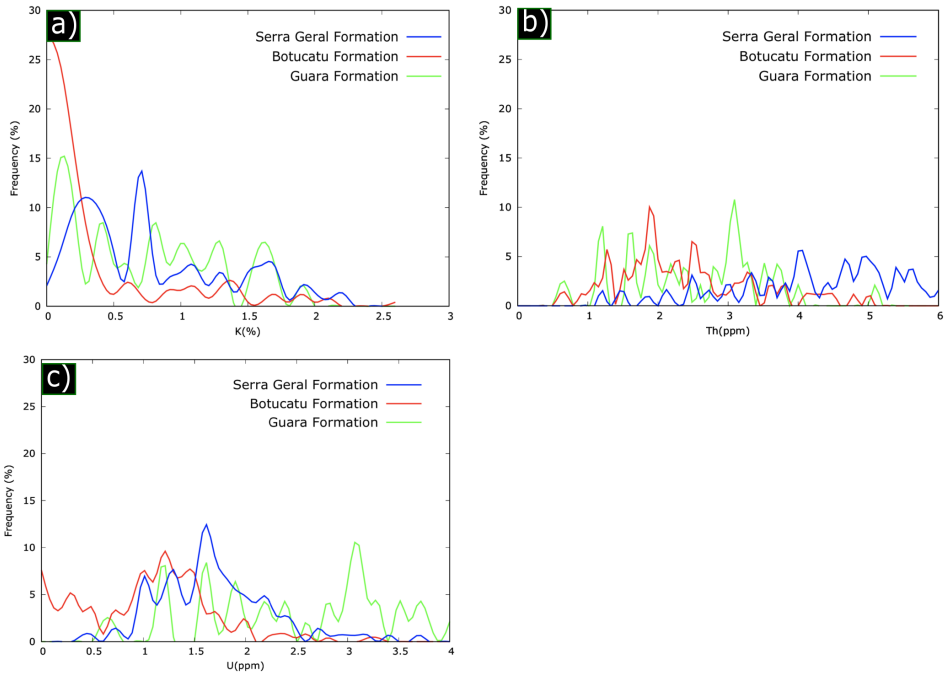

Figure 5. Frequency of detected values per lithology. In (a) K (%); (b) eTh (ppm); (c) eU (ppm).

These rocks show an average of 0.7% of K (Table II). According to Sánchez (2014), these are sub-alkaline basalts, comprised specially of andesitic basalts and andesites, therefore consistent with our gamma-ray data of the Garcia D.D. (unpublished data). Analysis of the frequency of K values in each geological unit is shown in Figure 5. It shows that areas with values of K > 1.5%, as observed over the Guará Formation, are less frequent in CJ (Figure 5a).

In the annular basin, eTh concentrations have an average of 6 ppm (Figure 4b). According to Dickson & Scott (1997), average eTh concentrations in soils over sandstones and shales are between 10-13 ppm. In the area of the central uplift, dominated by Guará and Botucatu Formations, eTh exhibits the lowermost concentrations, with values < 3 ppm. In Figure 5, the Botucatu sandstones show the highest frequency in comparison with the other lithologies in the low range of eTh, with a peak of 2 ppm. However, high values of eTh are clearly present in Botucatu sandstones of the southeastern area (red in Figure 4b).

eU concentration ranges from 0 to 4 ppm (Figure 4c) in CJ and in the surrounding areas. In the annular basin their values are heterogeneous, varying from 0 ppm in the western portion to 3 ppm, also occurring in a few places in the northern portion. Botucatu sandstones exhibit an average of 1.1ppm, and peak of ~1.6 ppm (Figure 5c). According to Crósta et al. (2010) and Sanchéz (2014), highly fractured and deformed sandstone grains are observed in Botucatu rock samples within CJ. In the central uplift, the eU distribution is irregular, ranging from 0 ppm in the eastern portion to 1.3 ppm in the western one, reaching up to 2 ppm in the central and northern areas with an average of 0.5. Because U is highly mobile and is absorbed onto the surfaces of clay particles and organic matter (e.g. Serra 1984), its concentration is higher when sandstones are intercalated with siltstones, compared to sandstone only. Figure 4c does not show difference between rocks of Guará and Botucatu formations. However, the elements'distribution show that the Botucatu Formation contains most frequencies in lower

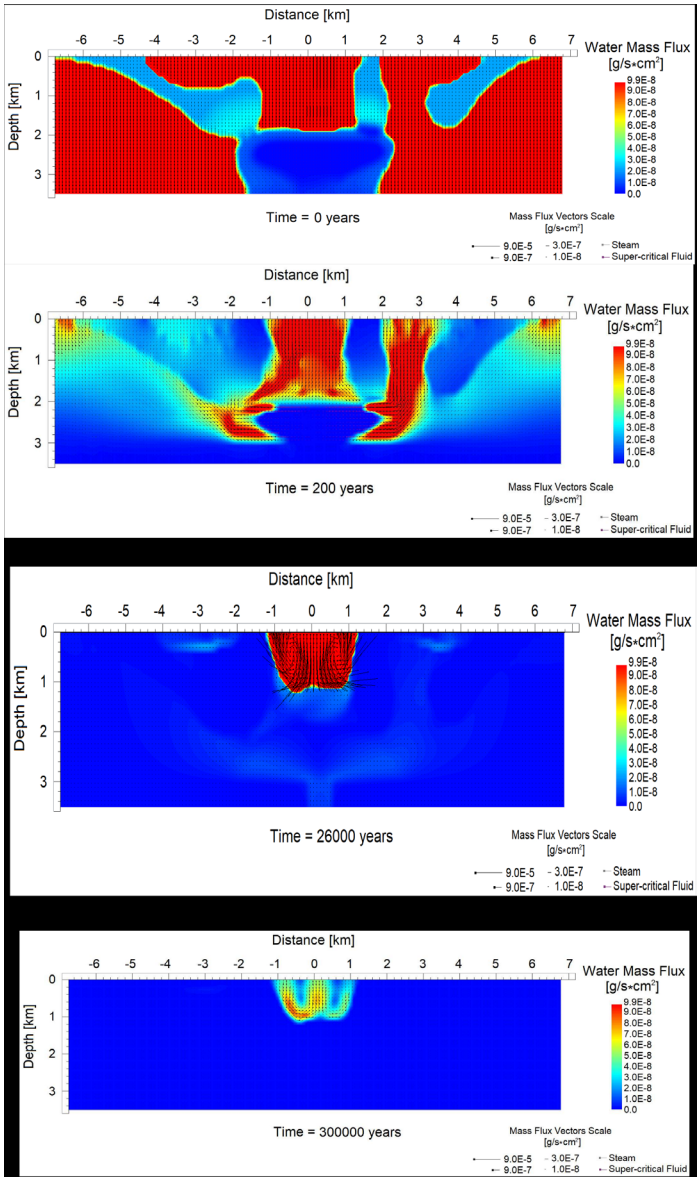

Figure 6. From top to bottom: time evolution of water (liquid), steam and super-critical fluid mass fluxes at the Cerro do Jarau structure after the impact. The estimated hydrothermal duration is of 300K - 320K years. Maximum mass flux is represented by values greater than 9.0E-8 g/s·cm² and shown in red colours within the geological domain, whereas negligible fluxes are illustrated in blue and concern estimates lower than 1.5E-8 g/s·cm². The presented simulation assumed lower permeability rock units and the lithostratigraphic distribution and boundary settings of scenario 5 (in supplementary materials).

ranges of eU, whereas the Guará Formation shows variations over the entire range (Figure 5c). The range is somehow within the range of ~2.1 ppm assumed by Dickson & Scott (1997) for soils over sandstones.

The eTh/K ratio (Figure 4d) ranges from 0.5 to 48. Contrasting eTh/K values are observed between the northern and southern portions of the area where the Botucatu sandstones occur. Ratio values are relatively low in the central part of the structure, over the sandstone of the Guará Formation, with an average of 3.7, due the high K concentrations. Outside the structure, it shows an average of 6.7.

HYDROTHERM Simulations

Since the post-impact hydrothermal activity in CJ has not been yet thoroughly investigated or/and established, the exploration of the post-impact cratering processes through numerical modeling considering the local geology should ideally follow a more conservative approach. The conservative sets of simulations for the analysis of hydrothermal circulation in CJ are

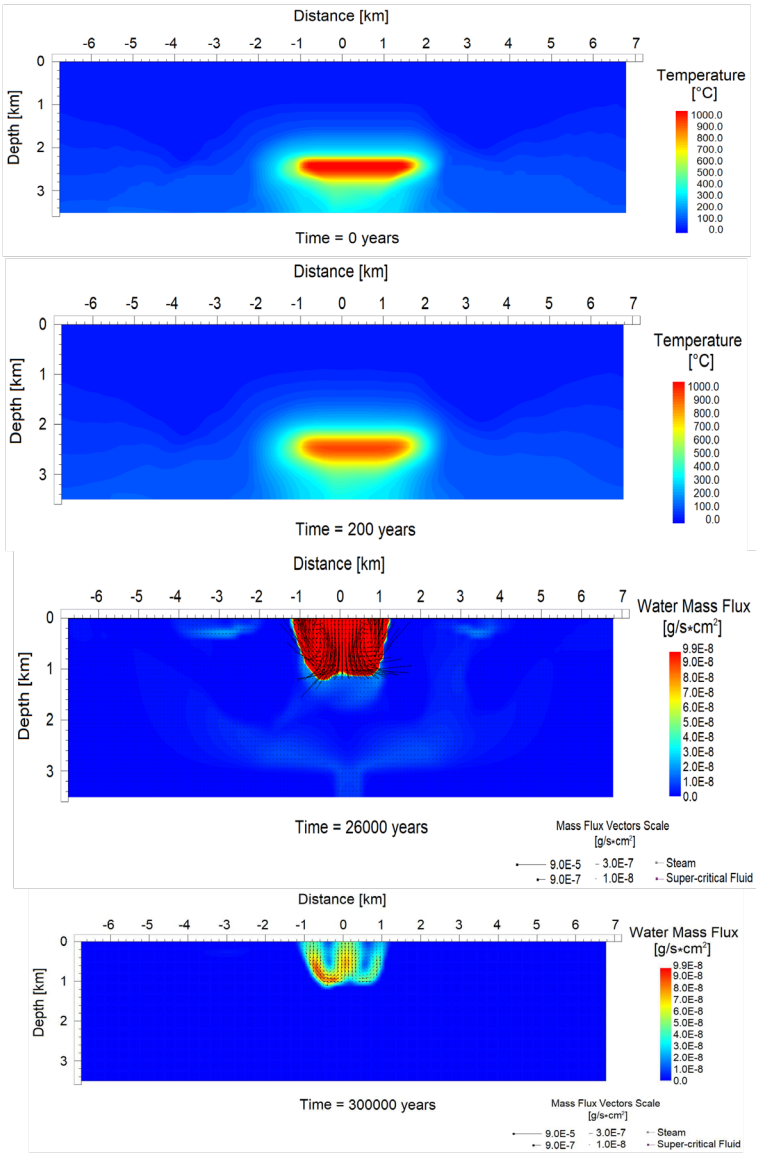

Figure 7. From top to bottom: the thermal evolution (cooling) over time at Cerro do Jarau after the crater's formation. Maximum temperatures at t=0 after the impact are T_{max} = 1000°C (shown in red; blue colours represent colder temperatures with T_{min} = 20°C). At 300K years after the impact, the geothermal gradient is restored and only some minor water fluxes are present within the central basin of the crater (black vectors with values of 3E-8 g/s·cm²) which disappear after 320K years (WMF_{max} = 1.5E-8 g/s·cm²). The presented simulation assumed lower permeability rock units and the lithostratigraphic distribution and boundary settings of the computational scenario 5 (in supplementary materials).

defined by the minimum permeability values for the specific lithologies.

By following this rationale, the numerical simulation that assumed the lowest permeability input values for all the modelled rock units should be considered as a conservative approach; meaning that this model should indicate the lower estimate for the duration of hydrothermal circulation. Moreover, in this research we emphasize more the low permeability scenarios, as these also seemed to yield more reliable and well-correlated results with the lithologies present in CJ. In the supplementary materials we have included all computational scenarios to compare the impact-induced hydrothermal circulation in CJ based on the different parameters and conditions (conservative versus liberal modelling approach, i.e.: low versus high permeability rocks, lower versus higher amount of basaltic mass in the geological domain according to the suggested rock distributions, presence versus absence of fluvial flows at the surficial sediments).

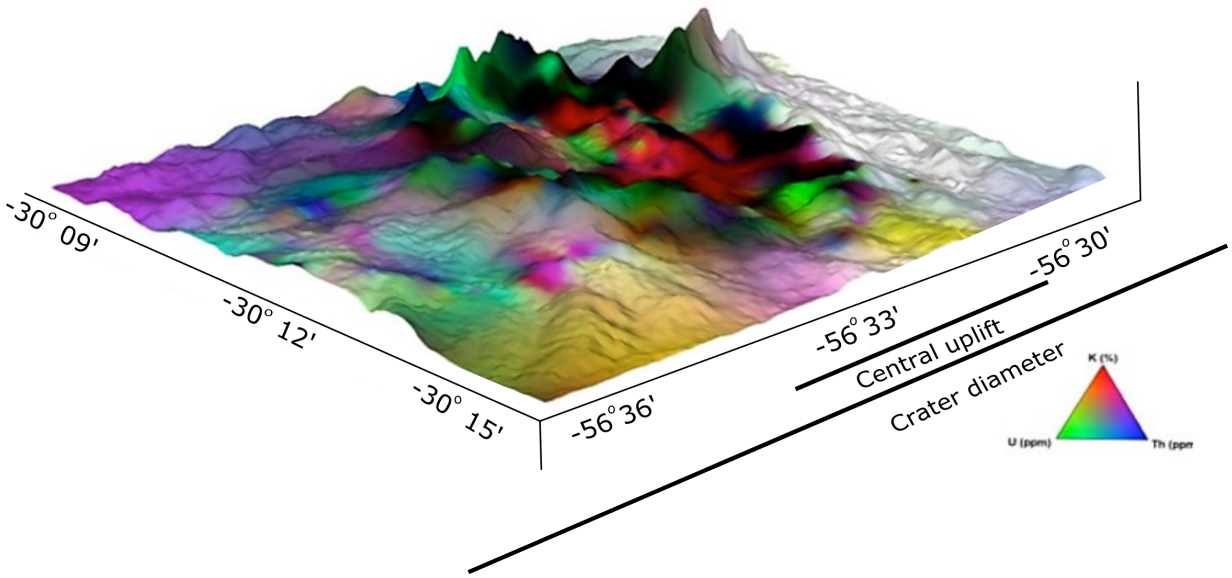

Figure 8. Gamma ternary map superposed to the SRTM topography model.

Figures 8 and 9 illustrate the evolution of the fluid mass flux and temperature in the CJ after the impact and for a period of 300K years, respectively. Initially, at t=0, we observe significant water mass fluxes (WMF) within the entire domain (red colour) with maximum values at circa 7.0E-4 - 9.0E-4 g/s·cm2. Induced steam and super-critical flows are present within the central heated region of the crater where the temperature is higher than 500° C, rendering this domain impermeable (dark blue region at t=0). In the impermeable overheated region, the two-phase and super-critical fluxes are smaller than the average water mass flux of the hydrothermal system by 3 orders of magnitude.

Additionally, although the basaltic rocks are not impermeable, they have lower permeability in comparison to all other rock units modelled. After 200 years, the maximum recorded temperature in our simulation grid has decreased by 15% and the WMFmax is smaller by an order of magnitude. The average water mass flux in the permeable regions of the crater has decreased by at least 60%. At 26k years after the impact, WMF within the broader lithostratigraphic reduces by almost an order of magnitude. At that point in time, we can observe some minor flows of ~1.5E-8 - 2.0E-8 g/s·cm2 at a depth of 2.5-3 km beneath the crater's central basin and within a radial distance of 3 km from the center, revealing two interconnected hydrothermal cells at the ending stage of their convective activity. Two slightly stronger hydrothermal cells are also observable in the outer-rim basin of the structure, although these seem to persist due to their recharge from surficial water.

On the other hand, at 26k years, it is evident that the fluvial-aeolian sediments and upper-impactites at shallow depths (z < 1km) and within a radius of 1.2 km from the center are hosting an appreciable convective cell, allowing fluid circulation to persist for a much longer time. As significant heat transfer from the impact-heated breccias and sandstones towards the surface occurs in the interval between 2 and 70k years (see Scenario 3; Figures S11, S12), the geothermal gradient becomes by three times greater at a depth of 1km and in a radius of 1km from the center and for a period greater than 70k years.

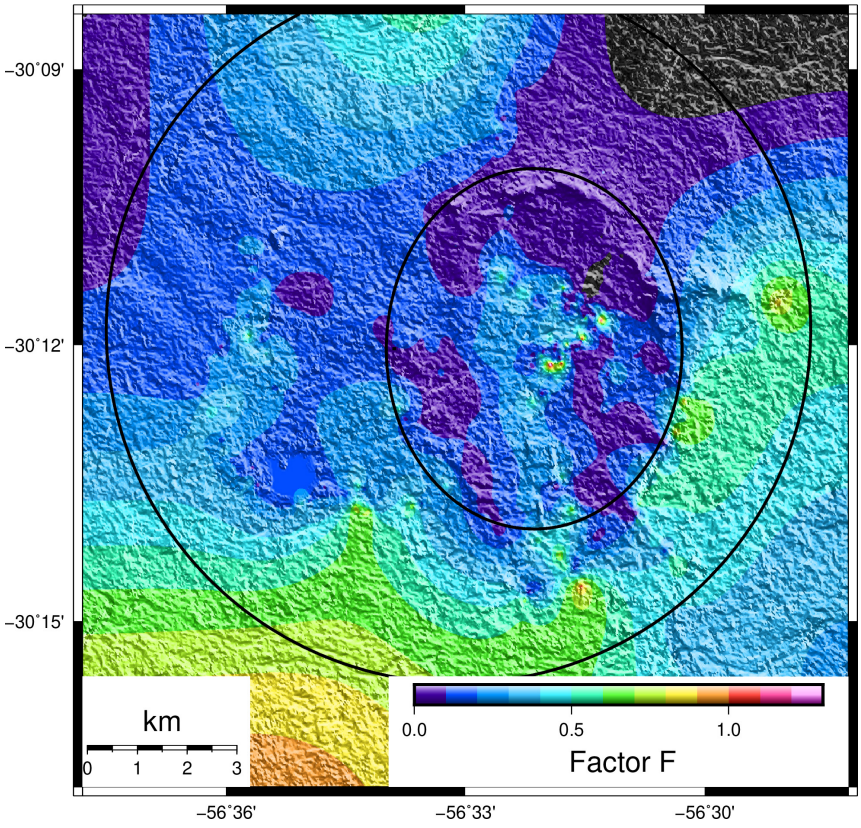

Figure 9. Factor F (%) image of the CJS. Black lines are the lithological contacts proposed by Crósta et al. (2010).

Beyond the outer-rim, the geothermal gradient is 1.5 times higher than the average value of 30 °C/km for a total period of 100k years after the impact. Then, the geothermal gradient appears fully restored and close to the pre-impact condition at ~300k years. According to our results, hydrothermal flows continue to exist in the interval between 70k and 300k years. After 300k years, all water circulation ceases, indicating the complete cooling of the hydrothermal setting.

DISCUSSION

The gamma-ray data show clear distinctions in the spatial distribution of K and eTh concentrations within CJ. Th concentrations are higher surrounding the central uplift area, whereas high K concentrations occur over the areas where the Guará Formation occurs and partially over the Botucatu Formation.

Galbraith & Saunders (1983) claim that Th enrichment generally does not accompany K enrichment in hydrothermal alteration processes, which means that their distinctive concentrations in the structure might be associated with different processes.

The ternary map showing the concentration of the three radiometric elements (Figure 8) depicts their spatial distribution and is helpful in determining their zonation. The overall high-K signature within the structure is remarkable, with an apparent relatively higher signature preferentially associated with the central uplift area. These high K values over the central area are similarly highlighted by the F-factor map (Figure 9). High K anomalies are commonly employed as an indication of hydrothermal enrichment (Efimov 1978, Pirajno 2005, Vasconcelos et al. 2012). This signature is consistent with the hypothesis of chemical elements' mobilization by hydrothermal flows

after the crater formation, causing enrichment in K. Indeed, the outcomes of our numerical modeling show that supercritical water flows have occurred in the structure's central area, especially in the innermost area (Figure 6). Supercritical flux in the HTI simulations represents water flows that are described by the low viscosity of a gas and the high density of a liquid, rendering such fluids difficult to liquify constituent components under any amount of given pressure. Supercritical water flows form in HTI simulations due to the immense pressure that is associated with the geostatic gradient and the excessive heat induced by the impact (i.e.: fluid's pressure > 220 bar, and 373 °C ≤ T_{fluid} ≤ 500 °C). Thus, regions of the simulated environment that seem to host supercritical water flows in the simulation imply that non-polar acidic fluids should have circulated therein. This observation from the model is consistent with the existence of high K concentrations in the area because the upper flow might drive such concentrations after 26k years. It also coincides with the presence of the impact-heated region in our simulations, which exhibits temperatures > 373 °C (third frame in Figure 7). Furthermore, the area surrounding the central region of the structure that is dominated by basalts shows the lowest permeability compared to the other lithologies. This explains why less intense water mass fluxes are associated with the basalt domain (average values up to 4.0x10-8 g/s·cm2).

By comparing the hydrothermal simulations in this low-permeability rock environment with the other modeled scenarios for the high-permeability cases presented in Supplementary Materials, and especially in the cases where there is contribution of cold inflows by streams at the surface and within the fluvial-aeolian deposits (scenarios: 2-4), we realize that in extremely high permeable lithologies (2 orders of magnitude greater), heat loss is somehow accelerated via the convective cooling case, and it is especially far more rapid via water upflow events towards the near-surface. This effect has been previously reported by Abramov & Kring (2004, 2005) and Jõeleht et al. (2005), and results in shorter lifetimes for the hydrothermal systems that undergo convective cooling, in contrast to those undergoing a conductive cooling process.

Our high-permeability geological setting is different only by an order of magnitude compared to the low-permeability setting and, hence, the cooling process and the lifetimes of the hydrothermal systems did not exhibit any substantial differences in the cooling pattern or/and the lifetime. In the higher-permeability case, just a prolonging effect for the duration of the hydrothermal system by 30-35k years was noticed. Numerical tests conducted after having assigned the permeability higher by 2 orders of magnitude resulted in a far more rapid cooling of the hydrothermal system, causing it to cease within 70K-100k years sooner than in the low-permeability case. Scenarios 3 and 4, presented as Supplementary Materials show similar results, where the steam influx contribution to the hydrothermal system renders it inactive much sooner, at ~200-250k years after the impact.

CONCLUSIONS

Our results point out the central uplifted core of CJ as characterized by high K concentrations, as shown by the gamma ray data and particularly highlighted by the Factor F map. Similarly, our numerical models show a robust convective hydrothermal flow system present in the center of the structure, which reinforces the concentration of K in this area. This system was established mainly due to the hot fluid circulation that likely took place throughout the rocks that form the central uplift during a period of ca. 26k years after the impact. Our

models also indicate that a relatively rapid post-impact cooling of the CJ impact structure is driven by convective heat transfer during the early phases of the post-impact stage. Most of the high post-shock temperatures in the central area decreased ~80% from their initial values only 26k years after the impact, depending on permeability. The system also changed from a dispersive flow throughout the crater into a convective heat transfer restricted to the center ~26k years after the impact. The thermal balance of the impact-heated rocks took much longer, with heat flow detectable until ~300k years after the impact event. A better characterization of the hydrothermal enrichment might be attained by adding mineralogical and geochemical information about the target rocks in future studies.

Acknowledgments

The authors are thankful to Fundação de Amparo à Pesquisa do Estado de São Paulo (FAPESP, grant #2014/13854-0) and Kenneth L. Kipp, Jr., Paul A. Hsieh, and Scott R. Charlton (USGS) for developing the version 3 of the HYDROTHERM code. D.D. Garcia is thankful to Conselho Nacional de Desenvolvimento Científico e Tecnológico (CNPq) for his undergraduate scholarship. E.V. Christou thanks the Leverhulme Trust Research Project Grant. A.P. Crósta acknowledges research grant #302679/2018-9, from the CNPq, Brazil.

REFERENCES

ABRAMOV O & KRING DA. 2004. Numerical modeling of an impact-induced hydrothermal system at the Sudbury crater. J Geophy Res 109 E10007.

ABRAMOV O & KRING DA. 2005. Impact-induced hydrothermal activity on early Mars. J Geophy Res 110 E12S09.

ABRAMOV O & KRING DA. 2007. Numerical modeling of impact-induced hydrothermal activity at the Chicxulub crater. Meteorit & Plan Sci 42: 93-112.

ALLEN CC, GOODING JL, & KEIL K. 1982. Hydrothermally altered impact melt rock and breccia: Contributions to the soil of Mars. J of Geophy Res: Solid Earth 87(B12): 10083-10101.

AMES DE, WATKINSON DH & PARRISH RR. 1998. Dating of a regional hydrothermal system induced by the 1850 Ma Sudbury impact event. Geol 26(5): 447-450.

BOANO F, HARVEY JW, MARION A, PACKMAN AI, REVELLI R, RIDOLFI L & WÖRMAN A. 2014. Hyporheic flow and transport processes: Mechanisms, models, and biogeochemical implications. Rev Geophy 52(4), p. 603-679.

BOROVIĆ S, POLA M, BAČANI A & URUMOVIC K. 2019. Constraining the recharge area of a hydrothermal system in fractured carbonates by numerical modelling. Geother 82: 128-149.

CRÓSTA AP. 2008. Basaltic impact structures of the Paraná Basin, Brazil. In Large Meteorite Impacts and Planetary Evolution IV, LPI Contribution Nº 1423, Lunar and Plan Inst, Houston, 58-59.

CRÓSTA AP, LOURENÇO FS & PRIEBE GH. 2010. Cerro Jarau, Rio Grande do Sul: a Possible New Impact Structure in Southern Brazil. In: Roger L, Gibson & Wolf U Reimold (Eds), Large Meteorite Impacts and Planetary Evolution IV. The Geol Soc of Am Spe Paper # 465.

EFIMOV AV. 1978. Multiplikativniyi pokazatel dlja vydelenija endogen- nych rud aerogamma-spectrometriceskim dannym. In: Metody rudnoj geofiziki. Leningrado, Naucno-proizvodstvennoje obj geofiz Ed 59-68.

FRENCH BM. 1998. Traces of catastrophe: A Handbook of Shock-Metamorphic Effects in Terrestrial Meteorite Impact Structures. LPI Contribution No. 954, Lunar and Planet Ins. Houston, 120 p.

FRENCH BM & KOERBEL C. 2010. The convincing identification of terrestrial meteorite impact structures: what works, what doesn't, and why. Earth Sci Rev 98: 123-170.

GALBRAITH JH & SAUNDERS DF. 1983. Rock classification by characteristics of aerial gamma ray measurements. J of Geoch Expl 18: 49-73.

GALLOWAY J, FOX A, LEWANDOWSKI J & ARNON S. 2019. The effect of unsteady streamflow and stream-groundwater interactions on oxygen consumption in a sandy streambed. Sci Reports 9(1): 19735.

GARCIA DD & LEITE EP. 2023. Ground Gamma-ray Spectrometry Data of the Cerro do Jarau Impact Structure [Data set]. Zenodo. https://doi.org/10.5281/zenodo.7891550.

GIACOMINI BB, LEITE EP & CRÓSTA AP. 2017. 3D gravimetric investigation of the Cerro do Jarau structure, Rio Grande do Sul, Brazil. Meteorit Plan Sci 52: 565-583.

GOMEZ-VELEZ JD, HARVEY JW, CARDENAS MB & KIEL B. 2015. Denitrification in the Mississippi River network controlled by flow through river bedforms. Nat Geosc 8: 941-945.

HAGERTY JJ & NEWSOM HE. 2003. Hydrothermal alteration at the Lonar Lake impact structure, India: Implications for impact cratering on Mars. Meteorit & Plan Sci 38(3): 365-381.

HAYBA DO & INGEBRITSEN SE. 1994. The computer model Hydrotherm, a three-dimensional finite-difference model to simulate ground-water flow and heat transport in the temperature range of 0 to 1,200 degrees C. 10.3133/wri944045 - USGS Publications Warehouse.

INGEBRITSEN SE & HAYBA DO. 1994. Fluid flow & heat transport near the critical point of H2O. Geoph Res L 21: 2199-2202.

JÕELEHT A, KIRSIMÄE K, PLADO J, VERSH E & IVANOV B. 2005. Cooling of the Kärdla impact crater: II. Impact and geothermal modeling. Met & Plan Sci 40: 21-33.

KRING DA, WHITEHOUSE MJ & SCHMIEDER M. 2021. Microbial sulfur isotope fractionation in the Chicxulub hydrothermal system. Astrob 21(1): 103-114.

LAMALI A ET AL. 2020, May. Gamma-ray spectrometry observations to monitor a presumed meteoritic signature at Maâdna crater (Talemzane, Algeria). In EGU Gen Ass Conf Abs, p. 2677.

LEITE EP, LAMBERT J, VASCONCELOS MAR, CROSTA AP & BATEZELLI A. 2022. Gamma-ray spectrometry of the Araguainha impact structure, Brazil: Additional insights into element mobilization due to hydrothermal alteration. An Acad Bras Cienc 94: e20210182. https://doi.org/10.1590/0001-3765202220210182.

MELOSH HJ & IVANOV B. 1999. Impact crater collapse. Annual Rev Earth Plan Sci 27: 385-415.

NAUMOV MV. 2002. Impact-generated hydrothermal systems: Data from Popigai, Kara, and Puchezh-Katunki impact structures. In Impacts in Precambrian Shields. Springer Berlin Heidelberg, p. 117-171.

NEWSOM HE, GRAUP G, SEWARDS T & KEIL K. 1986. Fluidization and hydrotermal alteration of the suevite deposit at the Ries crater, West Germany, and implications for Mars. J Geophy Res 91: 0148-0227.

NIANG CA ET AL. 2021. The Origin of the K-rich Annular Zones of the Bosumtwi Impact Structure: Insights of Radiometric Data and 10Be Analyses and Concentrations Simulations. AGU Meeting. New Orleans #P55C-1950.

OSINSKI GR. 2005. Shock-metamorphosed and shock-melted CaCO3-bearing sandstones from Haughton impact structure, Canada: Melting of calcite at ~10-20 GPa: Lunar and Plan Sci Conf, 36th, abstract 2038.

OSINSKI GR & SPRAY JG. 2001. Impact-generated carbonate melts: Evidence from the Haughton structure, Canada: Earth and Plan Sci L 194: 17-29.

PEATE DW. 1997. The Parana-Etendeka Province. In Large igneous provinces: Continental, oceanic, and planetary flood volcanism. In: Mahoney JJ & Coffin MF (Eds), Geophysical Monograph 100. Washington, D.C.: Am Geophy Union. pp. 217–245.

PIRAJNO F. 2005. Hydrothermal processes associated with meteorite impact structures: evidence from three Australian examples and implications for economic resources. Aus J Earth Sci 52(4-5): 587-605.

PIRAJNO F. 2009. Hydrothermal processes associated with meteorite impacts. Springer Netherlands, p. 1097-1130.

PIRES ACB. 1995. Identificação geofisica de áreas de alteração hidrotermal, Crixás-Guarinos, Goiás. Rev Br Geoc 25(1): 61-68.

PHILLIP RP, ROLIM SBA, SOMMER CA, SOUZA CR & LISBOA NA. 2010. A estrutura de impacto do Cerro do Jarau, Quaraí, RS. Rev Br Geoc, p. 468-483.

POELCHAU MH & KENKMANN T. 2011. Feather features: a low-shock-pressure indicator in quartz. J Geophy Res 116(B2).

PUURA V & PLADO J. 2004. Settings of Meteorite Impact Structures in the Svecofennian Crustal Domain. In: Koerberl C & Henkel H (Eds), Impact tectonics-Proceedings of the 8th. Workshop of the Euro Sci Found Sci Prog on the response of the Earth Sys to impact proc. Springer.

RATHBUN JA & SQUYRES SW. 2002. Hydrothermal Systems Associated with Martian Impact Craters. Icarus 157(2): 362-372.

REIMOLD WU, KOEBERL C, GIBSON RL & DRESSLER BO. 2005. Economic mineral deposits in impact structures: a review. Imp Tecto, Springer: 479-552.

REIMOLD WU, CRÓSTA AP, HASCH M, KOWITZ A, HAUSER N, SANCHEZ JP, SIMÕES LSA, DE OLIVEIRA GJ & ZAAG PT. 2019. Shock deformation confirms the impact origin for the Cerro do Jarau, Rio Grande do Sul, Brazil, structure. Meteorit Planet Sci 54: 2384-2397.

SÁNCHEZ JP. 2014. Mapeamento geológico – estrutural do astroblema de CJ – RS/Brasil. Tese de doutorado, UNESP Rio Claro, 178 p.

SÁNCHEZ JP, SIMÕES LSA & MARTINS LEB. 2014. Stratigraphy and structure of Cerro Jarau: New proposal. Br J Geol 44: 265-276.

SANFORD WE. 2005. A simulation of the hydrothermal response to the Chesapeake Bay bolide impact. Geofl 5: 185-201.

SCHERER CMS & LAVINA ELC. 2005. Sedimentary cycles and facies architecture of aeolian-fluvial strata of the Upper Jurassic Guará Formation, southern Brazil. Sedimen 52: 1323-1341.

SCHERER CMS & LAVINA ELC. 2006. Stratigraphic evolution of a fluvial-eolian succession: The example of the Upper Jurassic–Lower Cretaceous Guará and Botucatu Formations, Paraná Basin, southernmost Brazil. Gond Res 9: 475-484.

SCHMIEDER M & KRING DA. 2020. Earth's impact events through geologic time: A list of recommended ages for terrestrial impact structures and deposits. Astrobiol 20: 91-141.

SERRA O. 1984. The Acquisition of Logging Data: Part A. Elsevier.

SHIVES RBK, CHARBONNEAU BW & FORD KL. 2000. The detection of potassic alteration by gamma-ray spectrometry-Recognition of alteration related to mineralization. Geophy 65(6): 2001-2011.

TELFORD WM, GELDART LP & SHERIFF RE. 1990. Applied Geophysics. 2nd ed., Camb Uni Press, New York, 859 p.

THIELE DS & VASCONCELOS PM. 2010. Paraná flood basalts: Rapid extrusion hypothesis confirmed by new 40Ar/39Ar results. Geol 38: 747-750.

THOMS M, SCOWN M & FLOTEMERSCH J. 2018. Characterization of river networks: A GIS approach and its applications. J Am Water Res Ass 54(4): 899-913.

TIMMS N, ERICKSON TM, ZANETTI M, PEARCE MA, CAYRON C, CAVOSIE A, REDDY S, WITTMANN A & CARPENTER P. 2017. Cubic zirconia in >2370 °C impact melt records Earth's hottest crust. Earth Plan Sci L 477: 52-58.

VASCONCELOS MAR, LEITE EP & CROSTA AP. 2012. Contributions of gamma-ray spectrometry to terrestrial impact crater studies: The example of Serra da Cangalha, northeastern Brazil. Geophy Res L 39: L04306.

SUPPLEMENTARY MATERIAL

Figures S1-S17.

How to cite

GARCIA DD, LEITE EP, VASCONCELOS MAR, CHRISTOU E & CRÓSTA AP. 2024. Distribution of gamma-ray elements in Cerro do Jarau impact structure and a proposal of geothermal modeling. An Acad Bras Cienc 96: e20230005. DOI 10.1590/0001-3765202420230005.

Manuscript received on January 3, 2023;
accepted for publication on June 6, 2023

DIEGO D. GARCIA[1]
https://orcid.org/0000-0002-6824-4699

EMILSON P. LEITE[1]
https://orcid.org/0000-0003-1691-6243

MARCOS ALBERTO R. VASCONCELOS[2]
https://orcid.org/0000-0002-4970-0484

EVANGELOS CHRISTOU[3]
https://orcid.org/0000-0003-0601-7324

ALVARO P. CRÓSTA[1]
https://orcid.org/0000-0003-0485-1147

[1]Universidade Estadual de Campinas, Instituto de Geociências, R. Carlos Gomes, 250, Cidade Universitária, 13083-855 Campinas, SP, Brazil

[2]Universidade Federal da Bahia, Dep. de Geofisica, Instituto de Geociências, R. Barão de Jeremoabo, s/n, Ondina, 40170-290 Salvador, BA, Brazil

[3]University of Glasgow, College of Science & Engineering, School of Geographical & Earth Sciences, 27, Lilybank Gardens, Gregory Building, G12 8QW, Glasgow, Scotland

Author contributions

Diego Diez Garcia: Conceived the study, performed the gamma-ray data collection and analyses, draft the manuscript. Emilson Pereira Leite: Conceived the study, contributed to the conception, performed gamma-ray data collection and analyses, revised the manuscript and supervised the project. Marcos Alberto Rodrigues Vasconcelos: Contributed to the study and manuscript draft, data analyses and interpretation and revised the manuscript. Evangelous Christou: Conducted the HYDROTHERM simulations and interpretation. Alvaro Penteado Crósta: Supervised the manuscript writing and provided some insights.